Materials Today Sustainability 25 (2024) 100690

Contents lists available at ScienceDirect

Materials Today Sustainability

journal homepage: www.journals.elsevier.com/materials-today-sustainability

Enhancing catalytic and antibacterial activity with size-controlled yttrium and graphene quantum dots doped MgO nanostructures: A molecular docking analysis

Muhammad Abu Bakar Siddique [a], Muhammad Imran [a], Ali Haider [b], Anum Shahzadi [c], Anwar Ul-Hamid [d], Walid Nabgan [e,**], Malaika Batool [f], Karim Khan [g], Muhammad Ikram [f,***], H.H. Somaily [h], Asif Mahmood [i,*]

[a] Department of Chemistry, Government College University, Faisalabad, Pakpattan Road, Sahiwal, Punjab, 57000, Pakistan
[b] Department of Clinical Sciences, Faculty of Veterinary and Animal Sciences, Muhammad Nawaz Shareef, University of Agriculture, Multan 66000, Punjab, Pakistan
[c] Department of Pharmacy, COMSATS Islamabad, Lahore campus, 54000, Pakistan
[d] Core Research Facilities, King Fahd University of Petroleum & Minerals, Dhahran 31261, Saudi Arabia
[e] Departament d'Enginyeria Química, Universitat Rovira i Virgili, Av Països Catalans 26, 43007 Tarragona, Spain
[f] Solar Cell Applications Research Lab, Department of Physics, Government College University Lahore, Lahore 54000, Punjab, Pakistan
[g] International Collaborative Laboratory of 2D Materials for Optoelectronics Science and Technology of Ministry of Education, Institute of Microscale Optoelectronics, Engineering, Shenzhen University, Shenzhen, 518060, China
[h] Department of Physics, Faculty of Science, King Khalid University, P.O. Box 9004, Abha, Saudi Arabia
[i] Center for Clean Energy Technology, School of Mathematical and Physical Sciences, Faculty of Science, University of Technology Sydney, Sydney, 2007, Australia

ARTICLE INFO

Keywords:
Co-precipitation
GQDs
MgO
Active species
Molecular docking

ABSTRACT

Designing efficient catalysts that possess large number of active sites, high catalytic activity and selectivity while also exhibiting strong antimicrobial activity is a challenging task because of poor control over material fabrication. Therefore, developing new and innovative approaches for the synthesis of catalytic materials is crucial for addressing these challenges. Here, we report the controlled fabrication of GQDs/Y-doped MgO nanoparticles achieved by co doping of yttrium (Y) and graphene quantum dots (GQDs) in magnesium oxide (MgO) based nanostructures (NSs) using the co-precipitation method. The co-doping of GQDs and Y was controlled by manipulating the ratio of precursors where introduction of GQD resulted in higher surface area and enhanced conductivity while the doping of Y enhanced the number of active sites in the final product. The GQDs/Y-doped MgO exhibited an average particle size of ~50 nm and a bandgap of 3.6 eV. Owing to these excellent characteristics, the GQDs/Y-doped MgO was utilized as a catalyst for treatment of the organic pollutants from water as well as antibacterial activity. The modified GQDs/Y-doped MgO nanostructure exhibited excellent activity of over 99.9 % for dye removal and versatility in a broad range of pH which clearly indicated the application in a range of different environments. Furthermore, the GQDs/Y-doped MgO exhibited excellent antibacterial activity against *Escherichia Coli* (*E. Coli*) bacteria. To gain further insights into the origins of this excellent activity response, the molecular docking simulations (MDS) is utilized against DNA gyrase and FabI (two enzymes critical to nucleic acid and fatty acid biosynthesis, respectively), to uncover the mechanism behind the observed antibacterial effects. In summary, the modified catalyst provides a pathway to design highly efficient catalysts for all pH range water treatment as well as good activity against microbes.

* Corresponding author.
** Corresponding author.
*** Corresponding author.
E-mail addresses: walid.nabgan@urv.cat (W. Nabgan), dr.muhammadikram@gcu.edu.pk (M. Ikram), asif.mahmood@uts.edu.au (A. Mahmood).

https://doi.org/10.1016/j.mtsust.2024.100690
Received 14 October 2023; Received in revised form 24 December 2023; Accepted 28 January 2024
Available online 1 February 2024

1. Introduction

Water is a naturally occurring substance and plays a crucial role in the Earth's industrial and economic development. Despite the fact that water accounts for 71 % of the Earth's surface, only a fraction of it, just 0.03 %, is suitable for drinking, and this is typically derived from fresh groundwater, rivers, and lakes [1,2]. The environment has been significantly polluted by the presence of heavy metals and organic pollutants due to rapid industrialization and expanding human activities. Similarly, excessive usage of organic precursors in textile and pharmaceutical industries is contributing to the endangerment of aquatic life by allowing toxic dyes to proliferate [3]. The organic compounds such as dyes are directly discharged into water sources and ecosystems, resulting in severe environmental consequences by increasing the chemical oxygen demand for aquatic life [4]. The degradation of ecosystem leads to growth of microorganisms such as *Escherichia coli* (*E. coli*) in the water bodies which leads to proliferation of biological condition called mastitis. This is a prevalent production disease in dairy farms worldwide, resulting in chemical, physical, and bacteriological changes in milk due to mammary gland irritation [5,6]. Therefore, it is important to find ways to remove these pollutants from water to enable a sustainable environment.

Conventional methods, including ion exchange, adsorption, and aerobic treatment, are used to remove organic dyes from water. However, these methods have limitations and constraints, such as incomplete removal leading to dye transfer and secondary pollution, and high energy consumption [7,8]. Therefore, researchers are now focusing on the use of nanomaterials (NMs) as catalysts to remove the pollutants from water due to their low cost, less toxicity, chemical stability and environmentally friendly nature [9]. Among various metal oxides MgO, titanium dioxide (TiO_2), iron oxide (Fe_2O_3), tungsten oxide (WO_3), and zinc oxide (ZnO), MgO presents a very attractive material because of its ease of fabrication, non-toxicity and low-cost [10–12]. Over the years, several MgO nanostructures, such as nanoparticles, nanoflowers, and nanosheets have been designed and have shown promising activities for dye degradation, antibacterial properties, and adsorption capability [13]. MgO has been actively investigated among the known metal oxide nanoparticles due to its distinctive solid structure and novel applications in catalysis and antibacterial activity [14]. Research has shown that specific surface area and particle size are significant factors in the effectiveness of adsorption, where MgO has a surface area of 250–300 m^2/g and a zeta potential of approximately 29.89 mV [15]. Furthermore, according to the US Food and Drug Administration, nontoxic MgO has remarkable organic antibacterial applications for bone regeneration and heartburn relief compared to other Mg compounds [16–18]. Despite all these attractive features, the MgO based nanostructures still suffer from poor catalytic activity that must be improved to utilize these promising materials in practical applications.

Here, we utilize the concept of dual doping to improve the catalytic activity of the MgO nanostructures. The dual doping is achieved by introducing GQDs and the Y species. Carbon quantum dots (CQDs) have emerged in recent years as a potential class of carbon-based nanomaterials due to their excellent photo stability, water solubility, biocompatibility, and low toxicity [19]. The GQDs provide suitable substrates for anchoring of the MgO nanostructures resulting in higher surface area which eventually improves the contact area with the reacting species [20]. It has been demonstrated that the honeycomb sp^2-hybridized carbon structure of GQDs possesses excellent in vitro/-vivo biosecurity [21]. Since their initial discovery in 2004, GQDs have gained prominence ascribed to their adaptable structures, adjustable characteristics, superior water dispersibility, and remarkable compatibility with biological systems, rendering them highly suitable for numerous applications within the realm of biology [22,23]. The main advantage of Y doping is that it reduces the energy band gap. Surface enrichment of Y^{3+} inhibits crystallite development, while surface segregation of Y^{3+} promotes the formation of oxygen vacancies. Owing to the reasons above, Y doping is expected to boost degrading efficiency [24]. The Y doping introduces active sites with suitable binding energies for efficient catalytic response. The GQDs/Y-doped MgO is applied as a catalyst for removing organic dyes and as an antibacterial agent against *E. coli* bacteria [25]. The material was synthesized via the co-precipitation approach, and a range of characterizations were conducted to determine the impact of the dopant on the material's properties. The designed catalyst exhibits excellent antibacterial activity against *E. coli* as well as its efficacy in dye degradation. This study further highlights the potential of GQDs/Y-doped MgO as an inexpensive and environmentally friendly material for various applications, including wastewater treatment and medical uses.

2. Experimental Section

2.1. Materials

Magnesium chloride hexahydrate ($MgCl_2{\cdot}6H_2O$, 99.0 %), yttrium nitrate hexahydrate ($YN_3O_9.6H_2O$, 99.9 %), sodium hydroxide (NaOH, 98 %), glucose-D ($C_6H_{12}O_6$ 99.5 %), ammonia solution (NH_3, 33 %), and hydrochloric acid (HCl 37 %), were attained from Sigma Aldrich.

2.2. Synthesis of GQDs

GQDs were synthesized by 4g of glucose heated at 260 °C for 20 min until it was liquefied and yellow color turned orange. NH_3 solution (12.5 %) was incorporated dropwise to liquefied orange glucose and for 3 h vigorous stirring at 70 °C to eliminate ammonia odor. For neutral pH, HCl was incorporated. The obtained GQDs were stirred for 12 h at 150 °C and then ground into a very fine powder.

2.3. Synthesis of MgO and Y/GQDs-doped MgO

MgO and Y/GQDs nanostructures (NSs) were synthesized by the co-precipitation method. 0.25 M of $MgCl_2.6H_2O$ was stirred constantly at 80 °C for 1 h to synthesize MgO. Afterwards, $YN_3O_9.6H_2O$ (2, 4 wt %) as a source of Y and GQDs (2 %) were added in stirred solution, respectively. The pH was maintained at 12 by using 1 M of NaOH solution then precipitates were obtained. The solution was centrifuged two times with DI water to remove impurities at 15 °C, 7000 rpm for 7 min. Crystalloid solution was heated and stirred for 12 h at 80 °C, grinding the material into fine powder to obtain Y/GQDs doped MgO.

2.4. Catalytic activity

In catalytic activity, the oxidizing agent MB was degraded using sodium borohydride $NaBH_4$ and the previously synthesized NSs as catalysts. All reagents like $NaBH_4$ and MB have been utilized instantly after being prepared in order to preserve the experimental purity. Firstly, the MB solution was fabricated using 0.005 g of MB over 1000 mL of water and continuously stirred in the dark for 30 min. Utilizing a quartz cell, freshly synthesized 400 μL of 0.1 M solution of $NaBH_4$ was mixed with MB aqueous solution (3 mL). To prepare the nanocatalyst solution, 0.003 g of control and Y/GQDs doped MgO samples were dissolved in 3 mL of DI water and then 400 μL of this solution were added and well integrated with the solution. The progress was observed in the absorption reaction using a UV–Vis spectrophotometer at a specific time at normal temperature, in order to evaluate the rate at which MB dye degraded. When $NaBH_4$ was introduced, MB changed to its leuco form (LMB), exhibiting dye degradation.

2.5. Isolation and identification of MDR E. coli

2.5.1. Sample collection

Into sterile glassware, by direct milking, samples of raw milk were collected from lactating cows marketed at different vet clinics, markets

and dairy forms. After collection at 4 °C, raw milk was immediately transported to the laboratory. On MacConkey agar, coliforms in raw milk were numerated. For 48 h at 37 °C, all plates were incubated.

2.5.2. Identification and characterization of the bacterial isolates

Based on colonial morphology, *E. coli* was identified using the Gram stain and numerous biochemical assays in agreement with Bergey's Manual of Determinative Bacteriology [26].

2.5.3. Antibiotic susceptibility

The disc diffusion technique of Bauer et al. was used to conduct an antibiotics susceptibility test using Mueller Hinton agar (MHA) [27]. The test was carried out to explore antibiotic resistance of *E. coli*: Gentamicin (Gm) 10 μg (Aminoglycosides), Tetracycline (Te) 30 μg (Tetracyclines), Azithromycin (Azm) 15 μg (Macrolides), Ciprofloxacin (Cip) 5 μg (Quinolones), Amoxycillin (A) 30 μg (Penicillins), Ceftriaxone (Cro) 30 μg (Cephalosporins), and Imipenem (Imi) 10 μg (Carbapenem) [28]. *E. coli* purified cultures Growing and adjusting to the turbidity of 0.5 MacFarland. To avoid the inhibition zones from overlapping, the antibiotic discs were placed away from the surface of the inoculation plate on Muller Hinton Agar (MHA) (Oxoid Limited, Basingstoke, UK). The data was interpreted according to Laboratory and Clinical Standard Institute after incubating on plates for 24 h at 37 °C [29]. MDR was assigned to bacteria that were shown to be resistant to a minimum of three antibiotics [30].

2.5.4. Antimicrobial activity

Y/GQDs-doped MgO NSs were tested for antibacterial potential against germ strains derived from bovine and caprine mastitis. The potential in vitro antimicrobial activity of pure and Y/GQDs-doped MgO was examined using an agar well diffusion technique against ten chosen MDR *E. coli* isolates obtained from mastitic milk. A Petri dish containing Macconkey agar was swabbed with 1.5×10^8 CFU/mL (0.5 McFarland standard) MDR *E. coli*, and a sterilized cork borer was used to create 6 mm-diameter wells. The nanomaterials were used in various concentrations, including (1.0 mg/50 μL) and (0.5 mg/50 μL). For controls, the ciprofloxacin (0.005 mg/50 μL) was employed as the positive control, while DI water (50 μL) served as the negative control [31].

The Statistical analysis of inhibitory zone sizes, using SPSS 20, by one-way analysis of variance (ANOVA)and the bactericidal efficiency was estimated based on the size of the inhibitory zone (mm) [32].

2.6. Molecular docking analysis

Previously, it was believed that key enzymes in nucleic acid synthesis (i.e., Rifampicin's target) and fatty acid biosynthesis pathway were viable targets for the creation of antibiotics [33]. Antibiotics perform their function by targeting metabolic processes essential for bacterial survival and proliferation [34]. It is extensively reported that different metal-doped QDs possess bactericidal properties [35–37]. In this investigation, we utilized molecular docking (MD) to predict how DNA gyrase (i.e., the enzyme targeted by ciprofloxacin) and Enoyl-[acyl-carrier-protein] reductase (FabI) from the nucleic acid biosynthesis route and fatty acid metabolic pathway would react [38]. Accession codes 6KZV (Resolution: 2.4) and 4D46 (Resolution: 2.0) were obtained from the protein data bank to obtain the 3D crystal structures of the MDR *E. coli* target proteins, DNA gyrase and Enoyl-[acyl-carrier-protein] reductase (FabI), respectively [39,40]. We utilized the SYBYL-X 2.0 program to conduct docking investigations and evaluate the binding interactions between QDs and active site residues of the selected proteins, using the same methodology as in our prior research [41,42].

3. Results and discussion

The synthesis of GQDs using glucose as precursor material is shown in Fig. 1a. The growth of GQDs was done via a two-step methodology where the glucose was melted firstly followed by addition of ammonia solution to convert glucose into GQDs. The growth of GQDs was controlled by carefully controlling the addition of ammonia solution in glucose solution as well as maintaining the pH of the solution. The MgO nanostructures were pre-synthesized by co-precipitation method. The Y/GQD-doped MgO was synthesized by maintaining the concentration of GQD to a constant value and varying the Y concentration 2 and 4 wt. %. The synthesis methodology is summarized in Fig. 1.

XRD analysis was performed to examine the phase purity and structural properties of both pristine and doped MgO. The analysis was conducted over a range of 2θ values ranging from 10 to 80° and the results are presented in Fig. 2 (a). The diffraction peaks observed at 18.7°, 38.0°, 51.2°, 59.0°, and 62.5° along miller planes (001), (002), (012), (110), and (111), respectively, were in agreement with the hexagonal structure of MgO (h-MgO), as represented in Fig. 2a. The addition of GQDs led to a slight shift towards lower angles and broadening of the peaks, which could be attributed to the small dimensions of GQDs (less than 20 nm in diameter) and their high specific surface area [43]. Additionally, peak was observed at 32.0° (111), revealing the cubic structure of MgO (c-MgO) and peak at 27° ($\overline{20}$ 2) indicating monoclinic phase (*m*-$MgCO_3$), (JCPDS card no. 00-020-0669). The doping of Y into GQDs-MgO exhibited no new diffraction peaks clearly indicating that Y is doped in the crystal and no new phase was formed. However, relatively lower intensities show decreased crystal development and structural deformation caused by Y^{3+} ion exchange for the ion of the pure sample, which could result in oxygen vacancies [44]. The JCPDS card numbers 01-076-1363, 00-045-0946, 01-075-1525, and 96-901-3256 were used to match the patterns. A noticeable decrease in intensity at a higher Y percentage suggested a loss of crystallinity and a reduction in Y/GQDs-doped MgO NPs size [45].

The FTIR spectroscopy was used to identify functional groups and chemical compositions of modified materials. The results of the FTIR analysis of the MgO and Y/GQDs-doped MgO samples showed characteristic bands that corresponded to specific functional groups. The stretching vibration of H–O–H was detected at 3279 cm^{-1}, while the C═O stretching vibration was observed at 1381 cm^{-1}. The bands at 854 and 829 cm^{-1} were attributed to the vibration of Mg–O bonds [46,47]. The broadening of the bands in the doped samples was likely due to overlapping IR lines from both MgO and the dopant phase. Furthermore, the Selected-area electron diffraction (SAED) in Fig. 2c-f was used to obtain diffraction patterns for the modified samples to determine their crystal structures. The SAED analysis of the MgO and Y/GQDs-doped MgO samples showed discrete diffraction rings that were consistent with the planes (001), (200), (110), (111), (211), and (002) of MgO, confirming the XRD results.

The optical properties of the pristine and Y/GQDs-doped MgO were investigated using ultraviolet–visible (UV–vis) spectroscopy, as shown in Fig. 3a. The absorption band of MgO was observed at 250 nm associated with n-σ* transition [48] and pure GQDs showed absorption in the range of ~260–320 nm [49], inset in Fig. 3a. Upon doping with Y and GQDs, the intensity of the peak was enhanced, indicating an increase in absorption of the incident light indicating higher concentration of oxygen vacancies [50]. Tauc's equation was used to calculate the E_g that was decreased from (4.9–3.6 eV) for MgO and Y/GQDs doped MgO, respectively (Fig. 3b) and the band gap of GQDs 3.5 eV [51], inset in Fig. 3b. It is assumed that the value of E_g decreased because of an introduction of energy levels below and above the conduction band (CB) and valence band (VB), respectively, and increased oxygen vacancy concentration may be the source of the redshift [14]. Overall, the UV–vis spectroscopy results indicated that the Y/GQDs-doped MgO has improved optical properties compared to pristine MgO. Energy-dispersive X-ray spectroscopy (EDS) analysis was conducted to confirm the chemical composition of Y/GQDs doped MgO NSs, as shown in Fig. S1(a-d). The presence of O and Mg peaks confirmed the existence

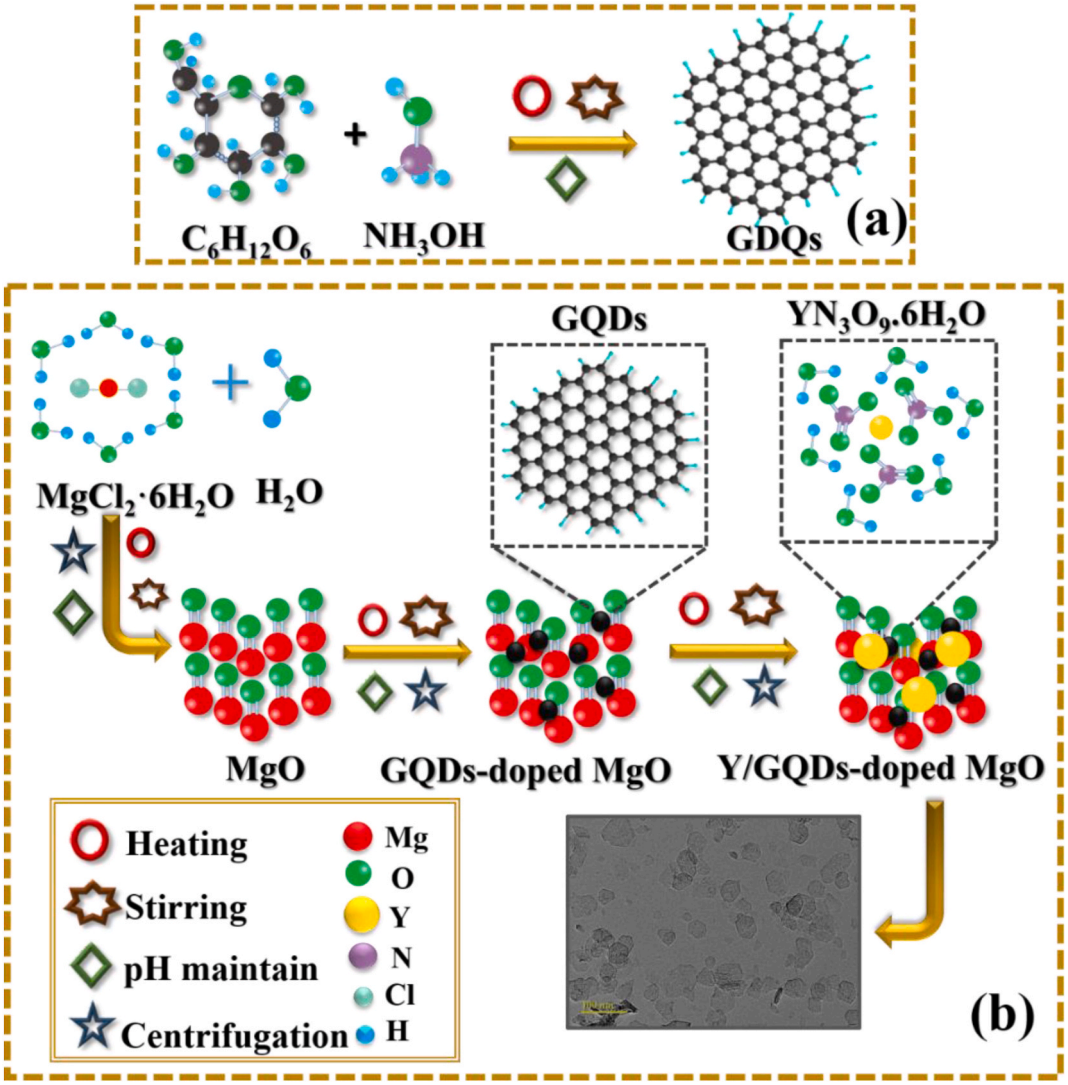

Fig. 1. Preparation of **(a)** GQDs **(b)** Y/GQDs doped MgO NSs, represented schematically.

of MgO, while the Y peak confirmed the doping of Y in the samples. The identified elements in Figs. S1e–j were uniformly distributed throughout the specimen levels, with varying elemental concentrations indicated by distinctive colors.

TEM micrographs (Fig. 4a–d) were used to analyze the structural and morphological characteristics of the synthesized MgO and Y/GQDs-doped MgO NSs. Fig. 4a shows multiple structures of MgO nanoparticles (NPs) with randomly oriented hexagonal and cubic-like structures. It can be seen that the average particle size of the MgO nanostructures is ~70–80 nm. Incorporation of GQDs on MgO NPs resulted in decrease of the particle size with overall small-sized agglomerated structures due to the two-dimensional QDs controlling the size of MgO (Fig. 4b). This reduction in particle size led to an increase in surface area, which enhanced the catalytic activity. The doping of 2 wt. % Y did not affect the particle size much as can be seen in Fig. 4c. However, increasing the dopant (Y) concentration to 4 wt. % resulted in random nanostructure with most of the particles having small particle size (Fig. 4d). The HR-TEM micrographs in Figs. S2a–d provided further morphological and structural information on the synthesized NSs. The calculated inter-layer spacing of MgO was found to be 0.14 nm, which was consistent with the XRD results (Fig. S2a). With the incorporation of Y and GQDs, the d-spacing value slightly increased to 0.17 and 0.23 nm, respectively, which agreed with the XRD results as the peaks shifted towards lower angles (Figs. S2b–d).

The catalytic reduction mechanism depicted in Fig. S3 involves the use of a reductant ($NaBH_4$) and is preferred for its recyclability, ease of use, and simplicity. The reactants ($NaBH_4$ and MB dye) adsorb onto the surface of the nanocatalyst, causing $NaBH_4$ to split into ionic species, with BH_4 acting as an H^+ and e^- donor species. In the catalytic reduction mechanism, $NaBH_4$ donates e^- and MB accepts electrons, resulting in the degradation of organic dye. The addition of a reducing agent without a nanocatalyst resulted in a prolonged reaction. The nanocatalyst accelerates the process by lowering the activation energy [52]. BH_4^- donates H^+ and e^- to MB dye, which breaks the double bond between aromatic rings and electrons. This results in conjugation, and the double-bonded N atom of the colorant molecule binds to the H atom, while the positively charged N accepts e^-. The nanocatalyst acts as an e^--transfer source between the reactants, allowing es^- to flow from the donor BH_4 atom and reducing MB to LMB. The presence of nanocatalysts accelerates the degradation efficiency.

The catalytic activity of the Y/GQDs-doped MgO NSs was found to be pH-dependent. The highest degradation rates were observed in the basic medium for all catalysts, with Y/GQDs-doped MgO NSs displaying the maximum catalytic activity. As shown in Fig. 5 (a-c), degradation rates of Y/GQDs in the acidic medium were 26, 95.74, 99.9, and 95.74 %; in the basic medium 13.6, 89.85, 99.9, and 99.9 %; and in the neutral medium 11.9, 63.36, 72.52, and 86.26 %, correspondingly, in 10 min. This is attributed to the cationic properties of MB, which promotes its

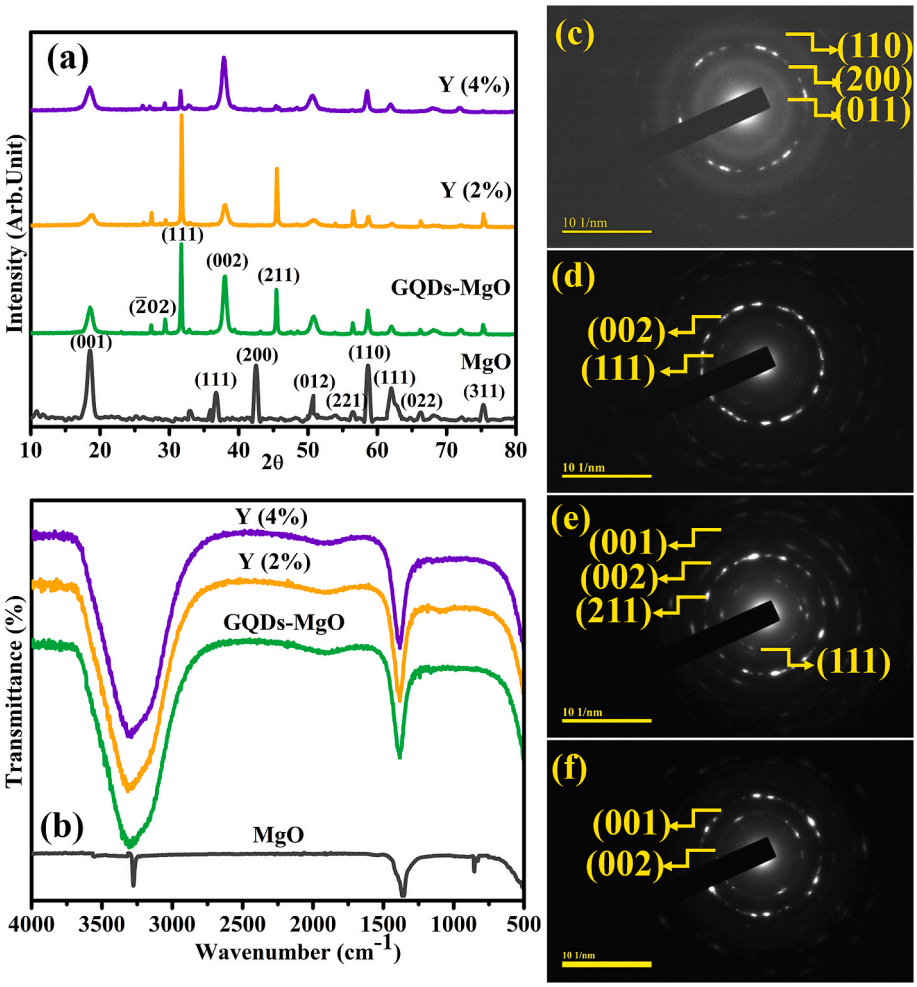

Fig. 2. **(a)** Diffraction pattern, **(b)** FTIR analysis, and **(c–f)** SAED pattern of MgO, GQDs-doped MgO, and Y (2 and 4 %) GQDs-doped MgO.

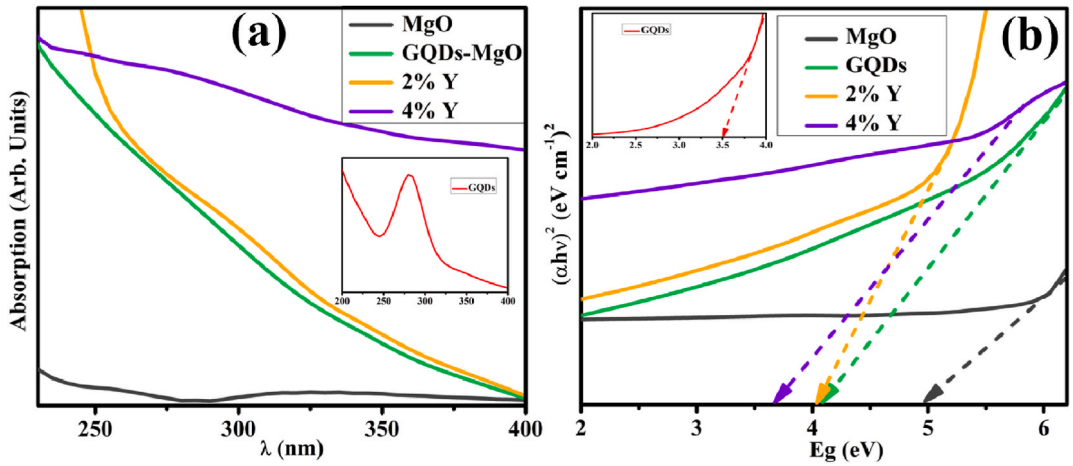

Fig. 3. **(a)** UV–Vis spectra and **(b)** E_g for MgO, GQDs-doped MgO, and Y (2 and 4 %) GQDs-doped MgO.

adsorption on the catalytic surface [53]. The research results revealed that the pH of the solution reaction constituted a vital role in dye degradation. But if the doping of Y^{3+} were increasing, Mg^{2+} concentration would surpass its optimal level and become the recombination center of electron-hole pairs, reducing catalytic activity [54]. The 4 % doping exhibited excellent activity in alkaline and neutral media owing to a larger number of active sites than undoped or 2 wt. % doped Y/GQDs doped MgO NSs. However, the 4 wt. % doped Y/GQDs doped MgO NSs seemed to have lower activity in acidic media in comparison to 2 wt. % doped Y/GQDs doped MgO NSs. It can be assumed that Y/GQDs doped MgO NSs with higher doping of Y may have degraded upon exposure to a highly corrosive acidic solution. The integration of GQDs in MgO NSs was found to enhance the degradation rate, attributed to the minimal size of the crystal and the extensive surface area of GQDs [43].

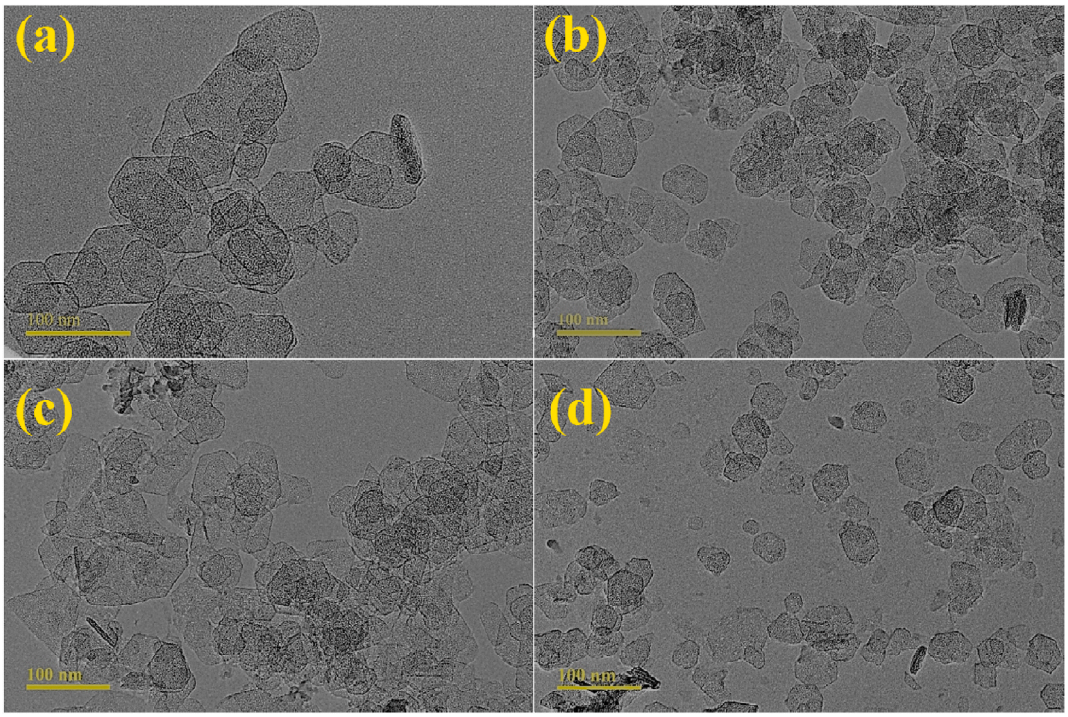

Fig. 4. TEM micrographs of **(a)** MgO, (b) GQDs-doped MgO, **(c)** 2 wt. %Y/GQDs doped MgO, **(d)** 4 wt. %Y/GQDs-doped MgO NSs.

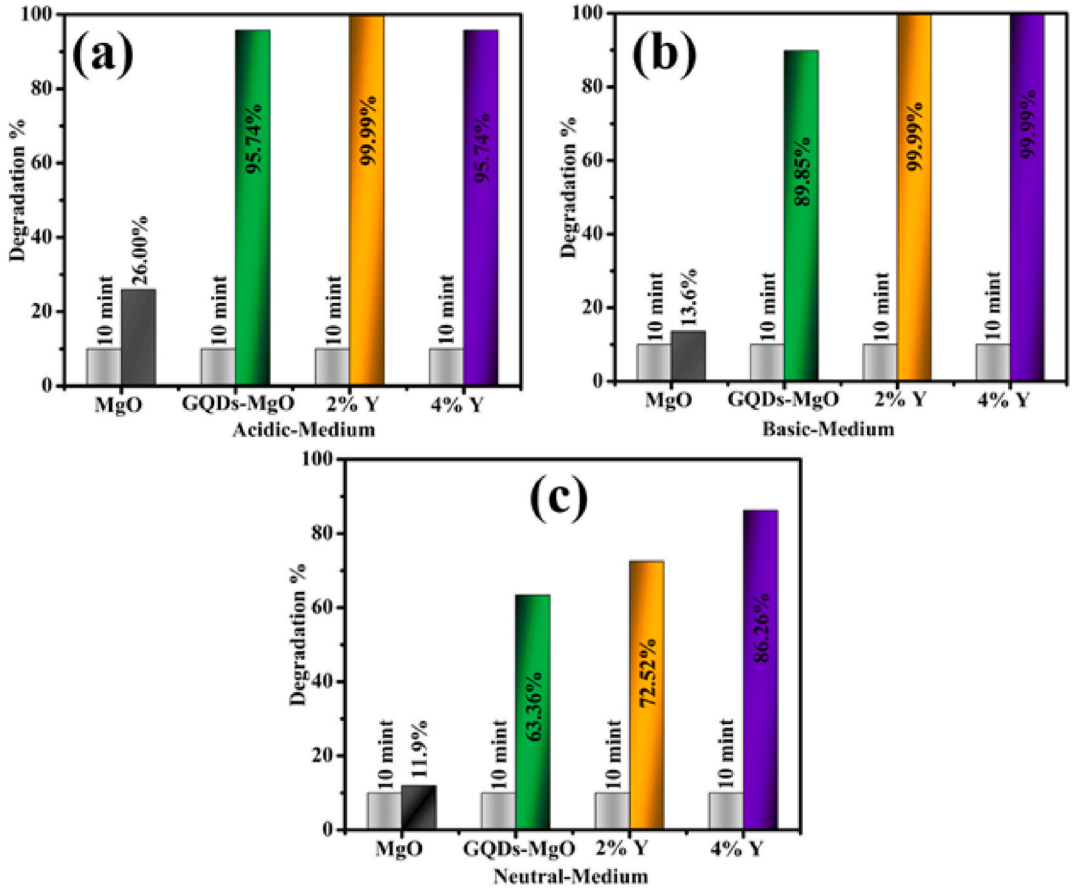

Fig. 5. Dye degradation of MgO, GQDs-doped MgO, and Y (2 and 4 wt. %) GQDs-doped MgO in (a) acidic, (b) basic, and (c) neutral media.

The Y doping further improved the catalytic activity due to the smaller crystallite size and effective dispersing of GQDs-doped MgO after Y doping, both of which contribute to the quantum-size effect [55].

The antibacterial activity of MgO and Y/GQDs-doped MgO NPs was investigated against *E. coli*, and the results are presented in Table 1. The inhibitory diameters in *E. coli* were found to be in the range of 1.55–2.85 mm to 2.05–4.95 mm at low and high doses, respectively. Pristine MgO showed lower activity against *E. coli* compared to Y/GQDs-doped MgO NPs, indicating that doping enhances antibacterial activity. The increased antibacterial activity of Y/GQDs-doped MgO NPs can be attributed to the smaller particle size and larger surface area, which allows for greater penetration into bacteria and destruction of their internal structures. In addition to particle size and surface area, the antibacterial activity was also affected by the cell surface charge density and the generation of free radicals and ROS (reactive oxygen species). The accumulation of NPs on the bacterial surface damages the cell membranes, leading to cell death by interfering with the reserve of NPs interruptions. The release of metal ions and ROS from NPs creates inhibitory zones that target the bacteria's DNA and proteins, denaturing their activity and ultimately leading to cell death (Fig. 6) [61]. Ciprofloxacin was used as a positive control, and its inhibitory diameter against *E. coli* was determined to be 8.65 mm, corresponding to 0 mm for DI water. This indicates that Y/GQDs-doped MgO NPs have comparable antibacterial activity to ciprofloxacin and can potentially be used as an alternative antibacterial agent (see Table 2).

In addition to their ability to bind with bacterial cells and disrupt cell membrane permeability, metal-doped QDs are also capable of interfering with important metabolic pathways [62]. Microbe toxicity of QDs is thus examined in more depth. Antibiotics may be able to battle bacterial infections by blocking enzymes that play a crucial role in bacterial survival, which is the infection's primary virulence factor [63]. On the basis of the good bactericidal activity (in vitro) of GQDs doped MgO and GQDs/Y- doped MgO against MDR *E. coli*, DNA gyrase and FabI enzymes of MDR *E. coli* were chosen as potential targets for molecular docking investigations (Fig. 7a and Fig. S4a). The optimal docked conformation of MgO doped with GQDs against DNA gyrase indicated an H-bonding interaction with Arg76 and a binding score of 1.49. (Fig. 7b). Fig. 7c shows that GQDs/Y-doped MgO had H-bonding interactions with Arg76 and Arg136 and a binding score of 3.37.

In the instance of FabI, the highest-scoring docked complex for MgO doped with GQDs demonstrated H-bonding interactions between Ala21 and Ser91 with a binding score of 3.36, as shown in Fig. S4b. Fig. S4c demonstrates that the GQDs/Y-doped MgO exhibited a binding score of 4.01 with H-bonding interactions with Ile20, Ala21, and Gly93.

4. Conclusions

In conclusion, this study demonstrates the successful synthesis of Y/GQDs doped-MgO NSs using a simple and environmentally friendly co-precipitation method. The material's structural and optical properties were characterized using various techniques, including TEM, FTIR, HRTEM, SAED, and UV–Vis spectroscopy. FTIR displayed Mg–O vibrations at 854 and 829 $cm^{-1,}$ and the elemental composition of as-prepared samples was analyzed by EDS mapping. D-spacing for Y/GQDs-doped MgO was investigated by HRTEM (0.14, 0.17 and 0.23 nm), respectively and crystalline behavior determined by SAED analysis. A UV–Vis spectrophotometer examined optical characteristics and a significant reduction in Eg (4.9–3.6 eV) attributed to doping. The results showed that the doping process reduced the bandgap of MgO, resulting in improved catalytic activity and bactericidal effectiveness against MDR *E. coli*. The in silico molecular docking simulations suggested the inhibition of DNA gyrase and FabI as the possible mechanism behind the material's biocidal activity. Overall, this study provides a promising approach for the development of efficient and sustainable antibacterial materials.

Table 2
Antibacterial efficacy of MgO and (2, 4 wt. %) Y/GQDs-doped MgO NSs.

Samples	Inhibition areas (mm)	
	0.5 mg/50 μL	1.0 mg/50 μL
MgO	1.55	2.05
GQDs-MgO	1.75	2.75
2 % Y	2.35	3.45
4 % Y	2.85	4.95
Ciprofloxacin	8.65	8.65
DI water	0	0

CRediT authorship contribution statement

Muhammad Abu Bakar Siddique: Data curation, Formal analysis, Investigation, Writing – original draft. **Muhammad Imran:** Formal analysis, Methodology, Validation, Writing – original draft, Writing – review & editing. **Ali Haider:** Conceptualization, Formal analysis, Investigation, Methodology, Writing – original draft. **Anum Shahzadi:** Formal analysis, Methodology, Validation, Visualization. **Anwar Ul-Hamid:** Data curation, Methodology, Resources, Writing – review & editing. **Walid Nabgan:** Investigation, Methodology, Supervision, Writing – review & editing. **Malaika Batool:** Investigation, Methodology, Validation, Writing – original draft. **Karim Khan:** Formal analysis, Methodology, Project administration, Visualization, Writing – original draft. **Muhammad Ikram:** Conceptualization, Funding acquisition, Supervision, Writing – original draft. **H.H. Somaily:** Investigation, Methodology, Writing – review & editing. **Asif Mahmood:** Conceptualization, Investigation, Methodology, Supervision, Writing – original draft, Writing – review & editing.

Declaration of generative AI and AI-assisted technologies in the writing process

During the preparation of this work the author(s) used AI in order to improve the language. After using this tool/service, the author(s) reviewed and edited the content as needed and take(s) full responsibility for the content of the publication.

Table 1
Comparative study about MB degradation of CSs/PAA-doped Al_2O_3 with previous literature.

Material	Synthesis route	Degradation method	MB degradation	References
Ag-Doped MgO Nanoparticles	Sol-gel	Photodegradation under UV irradiation	75 % in 180 min	[56]
Sn–MgO Nanoparticles	hydrothermal process	Photodegradation (UV light)	96 % in 200 min	[57]
MgO nanoparticles	co-precipitation method with annealing	Photodegradation under UV irradiation	79.05 % after 120 min	[58]
Cu-doped MgO nanoparticles	Sol–gel technique	Photodegradation (UV light)	90 % in 150 min along with cycling	[59]
MgO-0.6^{cc} OA nanostructures	ultrasound-assisted method	Photodegradation under visible light at optimum pH value	99 % in 25 min	[60]
GQDs/Y-doped MgO nanostructures	co-precipitation method	Catalytic degradation in the absence of light	99.99 % in 10 min	(present work)

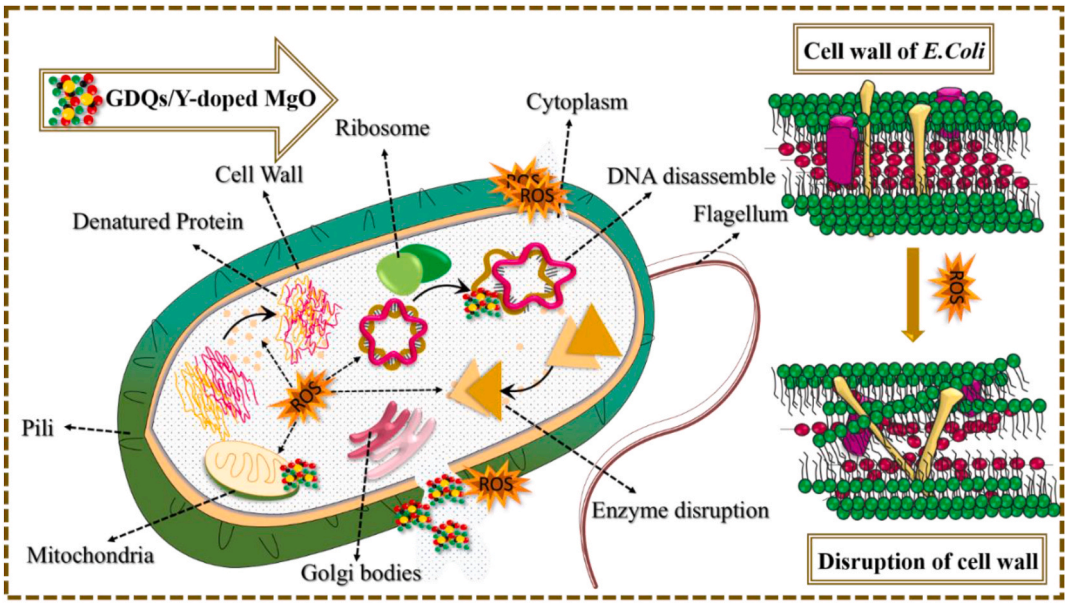

Fig. 6. Mechanism of antibacterial activity of prepared samples.

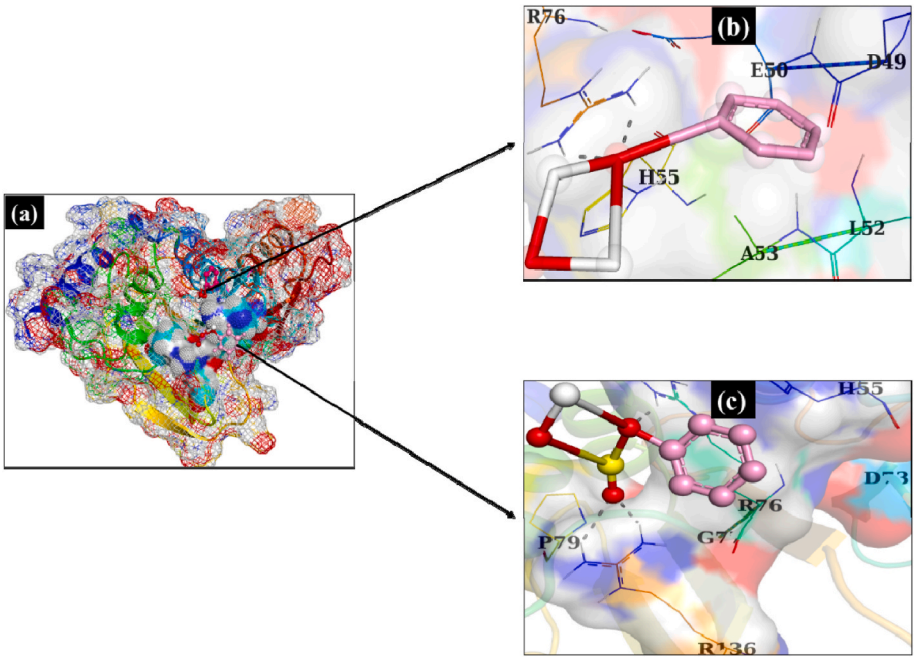

Fig. 7. Binding interaction analysis: (a) GQDs doped MgO and (b) Y/GQDs-doped MgO. The analysis were carried out with active site residues of DNA gyrase from MDR *E. coli*.

Declaration of competing interest

The authors declare no conflict of interest.

Data availability

Data will be made available on request.

Acknowledgements

The authors extend their appreciation to the Deanship of Scientific Research at King Khalid University for funding this work through large group Research Project under grant number (R.G.P.2/123/44). Authors are gratified to the Higher education commission (HEC) Pakistan through NRPU project-20-17615.

Appendix A. Supplementary data

Supplementary data to this article can be found online at https://doi.org/10.1016/j.mtsust.2024.100690.

References

[1] Z. Wang, A. Wu, L.C. Ciacchi, G. Wei, Recent advances in nanoporous membranes for water purification, Nanomaterials 8 (2018), https://doi.org/10.3390/nano8020065.

[2] M. Ikram, A. Raza, M. Imran, A. Ul-Hamid, A. Shahbaz, S. Ali, Hydrothermal synthesis of silver decorated reduced graphene oxide (rGO) nanoflakes with effective photocatalytic activity for wastewater treatment, Nanoscale Res. Lett. 15 (2020), https://doi.org/10.1186/s11671-020-03323-y.

[3] M. Heidarizad, S.S. Şengör, Synthesis of graphene oxide/magnesium oxide nanocomposites with high-rate adsorption of methylene blue, J. Mol. Liq. 224 (2016) 607–617, https://doi.org/10.1016/j.molliq.2016.09.049.

[4] A. Tkaczyk, K. Mitrowska, A. Posyniak, Synthetic organic dyes as contaminants of the aquatic environment and their implications for ecosystems: a review, Sci. Total Environ. 717 (2020) 137222, https://doi.org/10.1016/j.scitotenv.2020.137222.

[5] V.E. Ryman, N. Packiriswamy, L.M. Sordillo, Role of endothelial cells in bovine mammary gland health and disease, Anim. Health Res. Rev. 16 (2015) 135–149, https://doi.org/10.1017/S1466252315000158.

[6] T.A. Malik, M. Mohini, S.H. Mir, B.A. Ganaie, D. Singh, T.K. Varun, S. Howal, S. Thakur, Somatic cells in relation to udder health and milk quality-A review, J. Anim. Health Prod. 6 (2018) 18–26, https://doi.org/10.17582/journal.jahp/2018/6.1.18.26.

[7] H. Eccles, Treatment of metal-contaminated wastes: why select a biological process? Trends Biotechnol. 17 (1999) 462–465, https://doi.org/10.1016/S0167-7799(99)01381-5.

[8] S. Bhattacharya, I. Saha, A. Mukhopadhyay, D. Chattopadhyay, U. Chand, Role of nanotechnology in water treatment and purification: potential applications and implications, Int. J. Chem. Sci. Technol. 3 (2013) 59–64.

[9] M. Ali, S. Sharif, S. Anjum, M. Imran, M. Ikram, M. Naz, S. Ali, Preparation of Co and Ni doped ZnO nanoparticles served as encouraging nano-catalytic application, Mater. Res. Express 6 (2019), https://doi.org/10.1088/2053-1591/ab6383.

[10] S. Yang, P. Huang, L. Peng, C. Cao, Y. Zhu, F. Wei, Y. Sun, W. Song, Hierarchical flowerlike magnesium oxide hollow spheres with extremely high surface area for adsorption and catalysis, J. Mater. Chem. A 4 (2015) 400–406, https://doi.org/10.1039/c5ta08542j.

[11] Y. Zheng, L. Cao, G. Xing, Z. Bai, J. Huang, Z. Zhang, Microscale flower-like magnesium oxide for highly efficient photocatalytic degradation of organic dyes in aqueous solution, RSC Adv. 9 (2019) 7338–7348, https://doi.org/10.1039/C8RA10385B.

[12] H.L. Shuai, K.J. Huang, W.J. Zhang, X. Cao, M.P. Jia, Sandwich-type microRNA biosensor based on magnesium oxide nanoflower and graphene oxide–gold nanoparticles hybrids coupling with enzyme signal amplification, Sensor. Actuator. B Chem. 243 (2017) 403–411, https://doi.org/10.1016/j.snb.2016.12.001.

[13] M. Li, S. Zhou, M. Xu, Graphene oxide supported magnesium oxide as an efficient cathode catalyst for power generation and wastewater treatment in single chamber microbial fuel cells, Chem. Eng. J. 328 (2017) 106–116, https://doi.org/10.1016/j.cej.2017.07.031.

[14] M.R. Bindhu, M. Umadevi, M. Kavin Micheal, M.V. Arasu, N. Abdullah Al-Dhabi, Structural, morphological and optical properties of MgO nanoparticles for antibacterial applications, Mater. Lett. 166 (2016) 19–22, https://doi.org/10.1016/j.matlet.2015.12.020.

[15] E. Behzadi, R. Sarsharzadeh, M. Nouri, F. Attar, K. Akhtari, K. Shahpasand, M. Falahati, Albumin binding and anticancer effect of magnesium oxide nanoparticles, Int. J. Nanomed. 14 (2019) 257–270, https://doi.org/10.2147/IJN.S186428.

[16] P. Bhattacharya, S. Swain, L. Giri, S. Neogi, Fabrication of magnesium oxide nanoparticles by solvent alteration and their bactericidal applications, J. Mater. Chem. B 7 (2019) 4141–4152, https://doi.org/10.1039/c9tb00782b.

[17] V. Rajendran, B. Deepa, R. Mekala, Studies on Structural, Morphological, Optical and Antibacterial Activity of Pure and Cu-Doped MgO Nanoparticles Synthesized by Co-precipitation Method, I: Mater, Today Proc., 2018, https://doi.org/10.1016/j.matpr.2017.12.308 s. 8796–8803.

[18] K. Krishnamoorthy, J.Y. Moon, H.B. Hyun, S.K. Cho, S.J. Kim, Mechanistic investigation on the toxicity of MgO nanoparticles toward cancer cells, J. Mater. Chem. 22 (2012) 24610–24617, https://doi.org/10.1039/c2jm35087d.

[19] Z. Liu, W. Hou, H. Guo, Z. Wang, L. Wang, M. Wu, Functional group modulation in carbon quantum dots for accelerating photocatalytic CO_2 reduction, ACS Appl. Mater. Interfaces 15 (2023) 33868–33877, https://doi.org/10.1021/ACSAMI.3C05440/ASSET/IMAGES/LARGE/AM3C05440_0007.JPEG.

[20] M. Arvand, S. Hemmati, Analytical methodology for the electro-catalytic determination of estradiol and progesterone based on graphene quantum dots and poly(sulfosalicylic acid) co-modified electrode, Talanta 174 (2017) 243–255, https://doi.org/10.1016/j.talanta.2017.05.083.

[21] S. Yang, X. Wang, P. He, A. Xu, G. Wang, J. Duan, Y. Shi, G. Ding, Graphene Quantum Dots with Pyrrole N and Pyridine N: Superior Reactive Oxygen Species Generation Efficiency for Metal-Free Sonodynamic Tumor Therapy, Small 17 (2021) 2004867. https://doi.org/10.1002/smll.202004867.

[22] Y. Li, Z. Shi, L. Shang, Q. Tao, Q. Tang, H.J. Krause, S. Yang, G. Ding, H. Dong, Graphene quantum dots-based magnetic relaxation switch involving magnetic separation for enhanced performances of endoglin detection using ultra-low-field nuclear magnetic resonance relaxometry, Sensor. Actuator. B Chem. 380 (2023), https://doi.org/10.1016/J.SNB.2023.133389.

[23] Y. Li, P. Ma, Q. Tao, H.J. Krause, S. Yang, G. Ding, H. Dong, X. Xie, Magnetic graphene quantum dots facilitate closed-tube one-step detection of SARS-CoV-2 with ultra-low field NMR relaxometry, Sensor. Actuator. B Chem. 337 (2021), https://doi.org/10.1016/J.SNB.2021.129786.

[24] P.K. Sanoop, S. Anas, S. Ananthakumar, V. Gunasekar, R. Saravanan, V. Ponnusami, Synthesis of yttrium doped nanocrystalline ZnO and its photocatalytic activity in methylene blue degradation, Arab. J. Chem. 9 (2016) S1618–S1626, https://doi.org/10.1016/J.ARABJC.2012.04.023.

[25] K.V. Chandekar, T. Alshahrani, A. Ben Gouider Trabelsi, F.H. Alkallas, M. Shkir, S. AlFaify, Novel rare earth yttrium doping effect on physical properties of PbS nanostructures: facile synthesis and characterization, J. Mater. Sci. 56 (2021) 4763–4781, https://doi.org/10.1007/s10853-020-05539-w.

[26] C.G. Sinclair, Bergey's manual of determinative Bacteriology, Am. J. Trop. Med. Hyg. s1-19 (1939) 605–606, https://doi.org/10.4269/ajtmh.1939.s1-19.605.

[27] A.W. Bauer, W.M. Kirby, J.C. Sherris, M. Turck, Antibiotic susceptibility testing by a standardized single disk method, Am. J. Clin. Pathol. 45 (1966) 493–496, https://doi.org/10.1093/ajcp/45.4_ts.493.

[28] F. Adzitey, S. Yussif, R. Ayamga, S. Zuberu, F. Addy, G. Adu-Bonsu, N. Huda, R. Kobun, Antimicrobial susceptibility and molecular characterization of Escherichia coli recovered from milk and related samples, Microorganisms 10 (2022), https://doi.org/10.3390/microorganisms10071335.

[29] NCCLS, Performance standards for antimicrobial susceptibility testing, Clin. Lab. Standars Inst. - NCCLS. 27 (2007) 1–182.

[30] B.A. Iwalokun, A. Ogunledun, D.O. Ogbolu, S.B. Bamiro, J. Jimi-Omojola, In vitro antimicrobial properties of aqueous garlic extract against multidrug-resistant bacteria and Candida species from Nigeria, J. Med. Food 7 (2004) 327–333, https://doi.org/10.1089/jmf.2004.7.327.

[31] A. Haider, M. Ijaz, M. Imran, M. Naz, H. Majeed, J.A. Khan, M.M. Ali, M. Ikram, Enhanced bactericidal action and dye degradation of spicy roots' extract-incorporated fine-tuned metal oxide nanoparticles, Appl. Nanosci. 10 (2020) 1095–1104, https://doi.org/10.1007/s13204-019-01188-x.

[32] A. Haider, M. Ijaz, S. Ali, J. Haider, M. Imran, H. Majeed, I. Shahzadi, M.M. Ali, J. A. Khan, M. Ikram, Green synthesized phytochemically (zingiber officinale and allium sativum) reduced nickel oxide nanoparticles confirmed bactericidal and catalytic potential, Nanoscale Res. Lett. 15 (2020), https://doi.org/10.1186/s11671-020-3283-5.

[33] J.C. Priscu, B.C. Christner, Earth's Icy Biosphere, I: Microb. Divers. Bioprospecting, ASM Press, 2014, https://doi.org/10.1128/9781555817770.ch13 s. 130–145.

[34] J. Schiebel, A. Chang, S. Shah, Y. Lu, L. Liu, P. Pan, M.W. Hirschbeck, M. Tareilus, S. Eltschkner, W. Yu, J.E. Cummings, S.E. Knudson, G.R. Bommineni, S.G. Walker, R.A. Slayden, C.A. Sotriffer, P.J. Tonge, C. Kisker, Rational design of broad spectrum antibacterial activity based on a clinically relevant enoyl-acyl carrier protein (ACP) reductase inhibitor, J. Biol. Chem. 289 (2014) 15987–16005, https://doi.org/10.1074/jbc.M113.532804.

[35] M.S. Sharif, M. Aqeel, A. Haider, S. Naz, M. Ikram, A. Ul-Hamid, J. Haider, I. Aslam, A. Nazir, A.R. Butt, Photocatalytic, bactericidal and molecular docking analysis of annealed tin oxide nanostructures, Nanoscale Res. Lett. 16 (2021) 1–16, https://doi.org/10.1186/s11671-021-03495-1.

[36] M. Ikram, J. Hassan, A. Raza, A. Haider, S. Naz, A. Ul-Hamid, J. Haider, I. Shahzadi, U. Qamar, S. Ali, Photocatalytic and bactericidal properties and molecular docking analysis of TiO_2 nanoparticles conjugated with Zr for environmental remediation, RSC Adv. 10 (2020) 30007–30024, https://doi.org/10.1039/d0ra05862a.

[37] S. Altaf, A. Haider, S. Naz, A. Ul-Hamid, J. Haider, M. Imran, A. Shahzadi, M. Naz, H. Ajaz, M. Ikram, Comparative study of selenides and tellurides of transition metals (Nb and Ta) with respect to its catalytic, antimicrobial, and molecular docking performance, Nanoscale Res. Lett. 15 (2020), https://doi.org/10.1186/s11671-020-03375-0.

[38] D.M. Campoli-Richards, J.P. Monk, A. Price, P. Benfield, P.A. Todd, A. Ward, Ciprofloxacin, Drugs 35 (1988) 373–447, https://doi.org/10.2165/00003495-198835040-00003.

[39] J. Schiebel, A. Chang, B. Merget, G.R. Bommineni, W. Yu, L.A. Spagnuolo, M. V Baxter, M. Tareilus, P.J. Tonge, C. Kisker, C.A. Sotriffer, An ordered water channel in Staphylococcus aureus FabI: unraveling the mechanism of substrate recognition and reduction, Biochemistry 54 (2015) 1943–1955, https://doi.org/10.1021/bi5014358.

[40] F. Ushiyama, H. Amada, T. Takeuchi, N. Tanaka-Yamamoto, H. Kanazawa, K. Nakano, M. Mima, A. Masuko, I. Takata, K. Hitaka, K. Iwamoto, H. Sugiyama, N. Ohtake, Lead identification of 8-(Methylamino)-2-oxo-1,2-dihydroquinoline derivatives as DNA gyrase inhibitors: hit-to-lead generation involving thermodynamic evaluation, ACS Omega 5 (2020) 10145–10159, https://doi.org/10.1021/acsomega.0c00865.

[41] M. Ikram, K. Chaudhary, A. Shahzadi, A. Haider, I. Shahzadi, A. Ul-Hamid, N. Abid, J. Haider, W. Nabgan, A.R. Butt, Chitosan/starch-doped MnO_2 nanocomposite served as dye degradation, bacterial activity, and insilico molecular docking study, Mater. Today Nano. 20 (2022), https://doi.org/10.1016/j.mtnano.2022.100271.

[42] I. Shahzadi, M. Islam, H. Saeed, A. Haider, A. Shahzadi, J. Haider, N. Ahmed, A. Ul-Hamid, W. Nabgan, M. Ikram, H.A. Rathore, Formation of biocompatible MgO/cellulose grafted hydrogel for efficient bactericidal and controlled release of doxorubicin, Int. J. Biol. Macromol. 220 (2022) 1277–1286, https://doi.org/10.1016/j.ijbiomac.2022.08.142.

[43] M. Bacon, S.J. Bradley, T. Nann, Graphene quantum dots, Part. Part. Syst. Char. 31 (2014) 415–428, https://doi.org/10.1002/ppsc.201300252.

[44] A.B. Ali Baig, V. Rathinam, J. Palaninathan, Photodegradation activity of yttrium-doped SnO_2 nanoparticles against methylene blue dye and antibacterial effects, Appl. Water Sci. 10 (2020), https://doi.org/10.1007/s13201-020-1143-1.

[45] J. Yang, R. Wang, L. Yang, J. Lang, M. Wei, M. Gao, X. Liu, J. Cao, X. Li, N. Yang, Tunable deep-level emission in ZnO nanoparticles via yttrium doping, J. Alloys Compd. 509 (2011) 3606–3612, https://doi.org/10.1016/j.jallcom.2010.12.102.

[46] M. Sharma, P. Jeevanandam, Synthesis of magnesium oxide particles with stacks of plates morphology, J. Alloys Compd. 509 (2011) 7881–7885, https://doi.org/10.1016/j.jallcom.2011.04.151.

[47] M.H. Zahir, M.M. Rahman, K. Irshad, M.M. Rahman, Shape-stabilized phase change materials for solar energy storage: MgO and mg(OH)$_2$ mixed with polyethylene glycol, Nanomaterials 9 (2019), https://doi.org/10.3390/nano9121773.
[48] N. Pathak, P.S. Ghosh, S.K. Gupta, R.M. Kadam, A. Arya, Defects induced changes in the electronic structures of MgO and their correlation with the optical properties: a special case of electron-hole recombination from the conduction band, RSC Adv. 6 (2016) 96398–96415, https://doi.org/10.1039/c6ra21065a.
[49] S. Iravani, Green synthesis, biomedical and biotechnological applications of carbon and graphene quantum dots, R.V.-E. chemistry letters, undefined 2020, Rev. Springer Iravani, RS VarmaEnviron. Chem. Lett. 2020•Springer. 18 (2020) 703–727, https://doi.org/10.1007/s10311-020-00984-0.
[50] K.V. Chandekar, M. Shkir, A. Khan, M.A. Sayed, N. Alotaibi, T. Alshahrani, H. Algarni, S. AlFaify, Significant and systematic impact of yttrium doping on physical properties of nickel oxide nanoparticles for optoelectronics applications, J. Mater. Res. Technol. 15 (2021) 2584–2600, https://doi.org/10.1016/j.jmrt.2021.09.072.
[51] H.S. Al Ghamdi, A.A. Al-Ghamdi, Opening band gap of multi-color graphene quantum dots using D-fructose as a green precursor, Alex. Eng. J. 79 (2023) 155–163, https://doi.org/10.1016/J.AEJ.2023.08.019.
[52] A. Raza, J.Z. Hassan, M. Ikram, S. Naz, A. Haider, A. Ul-Hamid, I. Shahzadi, J. Haider, S. Goumri-Said, M.B. Kanoun, S. Ali, Molecular docking and DFT analyses of magnetic cobalt doped MoS_2 and BN nanocomposites for catalytic and antimicrobial explorations, Surface. Interfac. 27 (2021), https://doi.org/10.1016/j.surfin.2021.101571.
[53] A. Rafique, M. Ikram, A. Haider, A. Ul-Hamid, S. Naz, W. Nabgan, J. Haider, I. Shahzadi, Dye degradation, antibacterial activity and molecular docking analysis of cellulose/polyvinylpyrrolidone-doped cadmium sulphide quantum dots, Int. J. Biol. Macromol. 214 (2022) 264–277, https://doi.org/10.1016/j.ijbiomac.2022.06.058.
[54] X. Niu, S. Li, H. Chu, J. Zhou, Preparation, characterization of Y3+-doped TiO_2 nanoparticles and their photocatalytic activities for methyl orange degradation, J. Rare Earths 29 (2011) 225–229, https://doi.org/10.1016/S1002-0721(10)60435-8.
[55] Y. Wang, K. Lu, C. Feng, Photocatalytic degradation of methyl orange by polyoxometalates supported on yttrium-doped TiO_2, J. Rare Earths 29 (2011) 866–871, https://doi.org/10.1016/S1002-0721(10)60557-1.
[56] Z.M. Alaizeri, H.A. Alhadlaq, S. Aldawood, M.J. Akhtar, M.S. Amer, M. Ahamed, Facile synthesis, characterization, photocatalytic activity, and cytotoxicity of ag-doped mgo nanoparticles, Nanomaterials 11 (2021), https://doi.org/10.3390/nano11112915.
[57] M. Chandrasekar, M. Subash, V. Perumal, S. Panimalar, S. Aravindan, R. Uthrakumar, C. Inmozhi, A.B. Isaev, S. Muniyasamy, A. Raja, K. Kaviyarasu, Specific charge separation of Sn doped MgO nanoparticles for photocatalytic activity under UV light irradiation, Sep. Purif. Technol. 294 (2022), https://doi.org/10.1016/J.SEPPUR.2022.121189.
[58] P. Yadav, R. Saini, A. Bhaduri, Facile synthesis of MgO nanoparticles for effective degradation of organic dyes, Environ. Sci. Pollut. Res. 30 (2023) 71439–71453, https://doi.org/10.1007/S11356-022-21925-0.
[59] M. Subash, M. Chandrasekar, S. Panimalar, C. Inmozhi, K. Parasuraman, R. Uthrakumar, K. Kaviyarasu, Pseudo-first kinetics model of copper doping on the structural, magnetic, and photocatalytic activity of magnesium oxide nanoparticles for energy application, Biomass Convers. Biorefinery. 13 (2023) 3427–3437, https://doi.org/10.1007/s13399-022-02993-1.
[60] S. Fakhri-Mirzanagh, K. Ahadzadeh-Namin, G. Pirgholi Givi, J. Farazin, Y. Azizian-Kalandaragh, The effect of capping agent on the structural, optical properties and photocatalytic activity of MgO nanostructures, Phys. B Condens. Matter 583 (2020), https://doi.org/10.1016/J.PHYSB.2020.412064.
[61] M. Bilal, M. Ikram, T. Shujah, A. Haider, S. Naz, A. Ul-Hamid, M. Naz, J. Haider, I. Shahzadi, W. Nabgan, Chitosan-Grafted polyacrylic acid-doped copper oxide nanoflakes used as a potential dye degrader and antibacterial agent: in silico molecular docking analysis, ACS Omega (2022), https://doi.org/10.1021/acsomega.2c05625.
[62] A. Thill, O. Zeyons, O. Spalla, F. Chauvat, J. Rose, M. Auffan, A.M. Flank, Cytotoxicity of CeO_2 nanoparticles for Escherichia coli. Physico-chemical insight of the cytotoxicity mechanism, Environ. Sci. Technol. 40 (2006) 6151–6156, https://doi.org/10.1021/es060999b.
[63] I. Konieczna, P. Zarnowiec, M. Kwinkowski, B. Kolesinska, J. Fraczyk, Z. Kaminski, W. Kaca, Bacterial urease and its role in long-lasting human diseases, Curr. Protein Pept. Sci. 13 (2013) 789–806, https://doi.org/10.2174/138920312804871094.